

Efficient detection device for wafer physical defects

Jianyong Chen ¹, Xiaoyan Chen ^{1*}, Chundong Zhao ¹

¹ College of Electronic Information and Automation,
Tianjin University of Science and Technology, China;

E-mail: * cxywxr@tust.edu.cn

Www.tust.edu.cn

Abstract

Wafer defect detection is an important part of semiconductor manufacturing. In order to improve the efficiency of semiconductor wafer defect detection, this paper designs an efficient visual inspection device. The device uses programmable logic controller (PLC) as controller for the transmission mechanism and uses servo motor as drive device. A CMOS camera is used to capture wafer images, a computer is used for wafer image processing, and results are displayed on a graphical user interface. Camera calibration is implemented by integrating the mapping relationship between the pixel coordinate system and the world coordinate system, the internal and external parameters of the camera and the distortion coefficient. The device proposed in this paper is low in cost and the detection process is stable and reliable. It provides a new solution for wafer defect detection.

Keywords: Semiconductor manufacturing, Machine vision, Camera calibration, Programmable logic controller,

1. Introduction

Silicon wafer processing is the basis of semiconductor manufacturing. Wafer defect detection is one of the most important steps in semiconductor wafer manufacturing. Semiconductor wafer defect detection methods are mainly manual inspections, which are affected by human factors such as visual fatigue and are inefficient [1-3].

Research on the automatic wafer defect detection device was carried out to solve the problem of manual limitations in wafer defect detection. At present, with the development of machine vision technology, a large number of machine vision technologies have been used to detect chip shape, size, physical defects and other aspects [4-8].

The performance of wafer defect detection device directly affects the quality of semiconductor products and the efficiency of semiconductor testing [9-10]. In order to improve the detection efficiency and positioning accuracy of the automatic wafer defect detection device,

an optical system is designed and constructed in this paper to obtain a more complete wafer image. Camera calibration is used to eliminate the errors caused by the distortion of CMOS camera and improve the identification accuracy of the detection device. The main structure, motion mechanism, camera bracket and bearing platform of the device are designed and assembled. The Siemens s7-200 PLC is used as a controller to implement the control of all parts of the detection device.

2. Hardware Design

2.1. Dual-axes motion platform

The dual-axes(x-y) motion platform is selected for wafer defect detection. The horizontal ball screw pair of the platform is mounted on the longitudinal ball screw pair through the bracket, the longitudinal ball screw pair is directly mounted on the base surface, and the wafer stage is mounted on the horizontal ball screw pair through the

bracket. The lead screw pair is supported by both ends, and the drive motor and ball screw pair are directly connected. The assembly model is shown in Fig. 1.

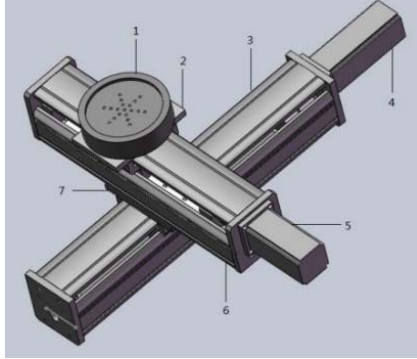


Fig. 1 Dual-axes motion platform. 1. Wafer stage 2. Bracket 3. Y-axis ball screw pair 4. Y-axis servo motor 5. X-axis servo motor 6. X-axis ball screw pair 7. Bracket

2.1.1.1. Ball screw pair

The ball screw pair is a transmission component that converts rotary motion into linear motion with high precision, high rigidity and high efficiency. Due to its low frictional resistance, ball screw pairs are widely used in a variety of industrial equipment and precision instruments.

The ball screw pair is rotationally driven by balls mounted between the spiral groove of the lead screw and the nut. According to the corresponding function, the ball screw pair is divided into four components, which are the screw, the nut, the ball and the reverser. In order to meet the requirements of positioning accuracy, feed rate, rapid response and stability of the motion platform, it is indispensable to choose a ball screw pair reasonably. The Y-axis ball screw pair is located in the lower layer with a larger load and higher precision requirements. Therefore, the Y-axis ball screw pair design parameters are used as the overall ball screw pair design index.

(i) Lead

The lead P_h is generally determined according to the maximum speed of the feed V_{max} , the maximum speed of the servo motor N_{max} and the transmission ratio i between the motor and the screw, which can be calculated by formula (1).

$$P_h = \frac{V_{max}}{i \times N_{max}} \quad (1)$$

In this paper, $V_{max} = 2400 \text{mm/min}$, $P_D = 5 \text{mm}$, $N_{max} = 480 \text{r/min}$.

(ii) Load and speed of ball screw pair

Equivalent load F_m is the actual axial force exerted on the ball screw by the transmission device. This device has no cutting operation, so equivalent load is equal to static friction force. F_m can be calculated by formula (2).

$$F_m = \mu \times (M_1 + M_2) \quad (2)$$

μ is the friction coefficient, the value is 0.04. M_1 is the X-axis ball screw counter gravity, about 80N. M_2 is the bearing table and the carrier table carrier gravity, about 20N. According to formula (2), F_m can be calculated as 0.4N.

(iii) Rated dynamic load

$$L_d = \left(\frac{C_{am} \times f_a \times f_c}{F_m \times f_w} \right) \times P_h \quad (3)$$

According to formula (3), rated dynamic load C_{am} can be calculated as 110N. L_d is the expected operating distance, $2.5 \times 10^8 \text{m}$. F_w is the load coefficient, set 1.0. f_a is the precision coefficient, set 1.0. f_c is the reliability coefficient, which is 0.62.

(iv) Ball screw subbottom diameter

Ball screw subbottom diameter d_{2m} can be calculated by the formula (4).

$$d_{2m} \geq 10 \sqrt{\frac{10F_0 \times L}{\pi \times \delta_m \times E}} \quad (4)$$

F_0 is the static friction of the guide rail. L is the distance between the support shafts at both ends. δ_m is the maximum allowable axial deformation of the ball screw. We figured out that d_{2m} is at least 0.43mm.

2.1.2. Servo motor

The device uses servo motor as the driving power system. The performance of the servo motor largely determines the positioning accuracy of the moving platform.

(i) Pulse equivalent

Pulse equivalent δ is the displacement of the actuator for each output pulse of the servo motor. It can be calculated from formula (5).

$$\delta = \frac{P_h \times i_m}{4i_n \times q} \quad (5)$$

i_m is the electronic gear ratio of servo motor, the value is 2.5. i_n is the transmission ratio. Since the motor shaft and lead screw are directly connected through the coupling, the value of i_n is 1. q is the resolution of servo motor encoder, the value is 2500 P/R.

(ii) Capacity and torque

When the motor is running, in order to ensure the stable operation of the system, the moment of inertia of the full equivalent load on the motor J should match the moment of inertia of the motor rotor J_m .

$$J_1 = \sum J_i \left(\frac{n_i}{n_m}\right)^2 + \sum m_1 \left(\frac{v_1}{2\pi \times n_m}\right)^2 \quad (6)$$

$$J = J_m + J_1 \quad (7)$$

Capacity and torque can be calculated from formula (6), (7). J_i and n_i are respectively the moment of inertia and speed of each rotating part. m_1 and v_1 are the mass and speed of each linear moving part respectively. J_m and n_m are the moment of inertia and speed of the motor respectively.

2.2. PLC controller

It is very important to select reliable and stable controller as the core of control system to ensure the stable and safe operation of transmission device. Programmable logic controller (PLC) is selected as the controller according to the requirements of the controlled object, so as to realize the effectiveness of the system. This paper follows the following PLC selection principles

- (i) Under the condition of meeting the requirement of the controlled object, the PLC controller can be used effectively.
- (ii) The control system has simple structure and strong maintainability.
- (iii) A certain amount of storage space and I/O points are reserved for subsequent adjustments and expansions.

According to the above requirements, Siemens s7-200 PLC, 224XP CN DC/DC/DC CPU were adopted in this paper.

3. Image acquisition system

The image acquisition system designed in this paper consists of CMOS industrial camera, lens and ring light source. CMOS industrial cameras transmit data in parallel for faster speeds. The purpose of a lens is to image an object optically onto a sensor. The diameter of the ring light source is 100mm-140mm, which is used to make the image receiving light uniform and clear. The structure of the image acquisition system is shown in Fig.2

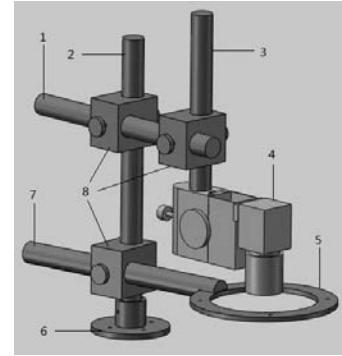


Fig. 2 Image acquisition system. 1. Camera shaft 2. Spindle 3. Camera shaft 4. CMOS camera 5. Light source fixing ring 6. Flange base 7. Light source shaft 8. Fixture

4. Camera Calibration

The main role of camera calibration is to correct image distortion and determine the positional relationship between the pixel coordinate system and the world coordinate system.

4.1. Calibration principle

(i) Camera internal and external parameters
As shown in formula (8), (9), The default value of Z plane is 0. φ is the scale factor. A is the internal parameter matrix. f_x, f_y is the scale factor of the u-axis and v-axis of the pixel coordinate system. γ represents the scale deviation of pixel points in the image coordinate system. u_0 and v_0 are the center of the image plane. r_1, r_2 and t are rotation matrix and translation vectors respectively.

$$\varphi \begin{bmatrix} u \\ v \\ 1 \end{bmatrix} = A[r_1, r_2, t] \begin{bmatrix} X \\ Y \\ 1 \end{bmatrix} \quad (8)$$

$$A = \begin{bmatrix} f_x, \gamma, u_0 \\ 0, f_y, v_0 \\ 0, 0, 1 \end{bmatrix} \quad (9)$$

As shown in formula (10), (11), (12), H is a homography matrix, and the basic constraint condition of internal parameter matrix can be deduced according to the properties of rotation matrix. The homography matrix can be obtained by the least square method with the pixel coordinates and world coordinates of the detected corner points.

$$H = [h_1, h_2, h_3] = A[r_1, r_2, t] \quad (10)$$

$$\begin{cases} r_1 = A^{-1}h_1 \\ r_2 = A^{-1}h_2 \end{cases} \quad (11)$$

$$\begin{cases} h_1^T A^{-T} A^{-1} h_2 = 0 \\ h_1^T A^{-T} A^{-1} h_1 = h_2^T A^{-T} A^{-1} h_2 \end{cases} \quad (12)$$

(ii) Camera distortion factor

Ideally, the least square method can be used to calculate the camera distortion coefficient according to formula (13) (14) (15). Ideally (no distortion), the pixel coordinates are (u, v), and the coordinates in the image coordinate system are (x, y). When there is distortion, the real pixel coordinates are (\bar{u}, \bar{v}), and the coordinates in the image coordinate system are (\bar{x}, \bar{y}).

$$\begin{cases} \bar{x} = x + x(k_1(x^2 + y^2) + k_2(x^2 + y^2)^2) \\ \bar{y} = y + y(k_1(x^2 + y^2) + k_2(x^2 + y^2)^2) \end{cases} \quad (13)$$

$$\begin{cases} \bar{u} = u + (u - u_0)(k_1(x^2 + y^2) + k_2(x^2 + y^2)^2) \\ \bar{v} = v + (v - v_0)(k_1(x^2 + y^2) + k_2(x^2 + y^2)^2) \end{cases} \quad (14)$$

$$\begin{bmatrix} (u - u_0)(x^2 + y^2), (u - u_0)(x^2 + y^2)^2 \\ (v - v_0)(x^2 + y^2), (v - v_0)(x^2 + y^2)^2 \end{bmatrix} \begin{bmatrix} k_1 \\ k_2 \end{bmatrix} = \begin{bmatrix} \bar{u} - u \\ \bar{v} - v \end{bmatrix} \quad (15)$$

4.2. Calibration results

By using a standard checkerboard, the camera takes pictures of the imaging area from different angles to obtain a set of calibration images. The image corner information is extracted, and the internal parameters, external parameters and distortion coefficients of the camera are obtained by the mapping relationship between the pixel coordinates of the corner points and the corner coordinates of the world coordinate system.

In this paper, 7×9 black and white checkerboard grids are selected, and the size of each grid is 8mm×8mm. A total of 9 standard checkerboard grid images are collected for calibration. According to formula (10)-(15), the internal parameter matrix A and distortion coefficients dist are obtained as follows:

$$A = \begin{bmatrix} 26704.79043, & 0, & 1384.94299 \\ 0, & 26754.77535 & 1415.48126 \\ 0, & 0, & 1 \end{bmatrix}$$

$$\text{dist} = \begin{bmatrix} 1.18344 \\ -1034.57967 \\ 0.02802 \\ 0.01921 \\ -6.37039 \end{bmatrix}$$

The maximum calibration error is $\delta_{max}=0.2125\text{pix}$, and the average error is $\delta_{ave} = 0.193048\text{pix}$.

5. Acknowledgement

The authors would like to appreciate for the financial support from Tianjin Municipal Science and Technology Bureau (Grand NO.18YFZCGX00360) and from the National Natural Science Foundation of China (Grand NO.61903274 and NO.41704131), the same appreciate for Tianjin FLY Tech Co., Ltd for offering samples and for Intelligent Edge Computing Joint LAB of TUST for the testing result analyzing.

References

1. Zhou, Q. and B. Zhou, An impending deadlock-free scheduling method in the case of unified automated material handling systems in 300 mm wafer fabrications[J]. Journal of Intelligent Manufacturing. Jan 2018, Vol. 29 Issue 1, pp. 155.
2. Tirkel, I., The efficiency of inspection based on out of control detection in wafer fabrication[J]. Computers & Industrial Engineering. Sept, 2016, Vol. 99, pp. 458.
3. Stefan Bengtsson, "Semiconductor Wafer Bonding - A Review Of Interfacial Properties And Applications[J]" Journal Of Electronic Materials, 1992, vol. 21, no. 8, pp. 841-862.
4. Wenjun, Liu, Thermography techniques for integrated circuits and semiconductor devices[J]. Sensor Review, 2007, Vol. 27, Issue 4, pp. 298-309.
5. Amatya, S, Automated Detection of Branch Shaking Locations for Robotic Cherry Harvesting Using Machine Vision[J]. Robotics, 2017, Vol 6, Issue 4, pp 31.
6. Binch, A. and C.W. Fox, Controlled comparison of machine vision algorithms for Rumex and Urtica detection in grassland[J]. In Computers and Electronics in Agriculture August 2017, 140:123-138.
7. Huang, B, Full Length Article: Research and implementation of machine vision technologies for empty bottle inspection systems[J]. In Engineering Science and Technology, an International Journal February 2018, 21(1):159-169.
8. Eguiraun, H., O. Casquero and I. Martinez, The Shannon Entropy Trend of a Fish System Estimated by a Machine Vision Approach Seems to Reflect the Molar Se:Hg Ratio of Its Feed[J]. Entropy, 2018, Vol 20, Issue 2, pp. 90.
9. Joy, J, Capacitance-voltage profiling of MOS capacitors: A case study of hands-on semiconductor testing for an undergraduate laboratory[J], American Journal of Physics, Oct,2018, Vol. 86 Issue 10, pp 787-796.
10. Wang, K.J, T.C. Hou, Modelling and resolving the joint problem of capacity expansion and allocation with multiple resources and a limited budget in the semiconductor testing industry[J], International Journal of Production Research, 2003, Vol. 41 Issue 14, pp 217-3235.